Computational Design of SCS Nickel Pincer Complexes for the Asymmetric Transfer Hydrogenation of 1-Acetonaphthone

Bing Qiu [1,2] , **Wan Wang** [1,2] **and Xinzheng Yang** [1,2,*]

1   Beijing National Laboratory for Molecular Sciences, State Key Laboratory for Structural Chemistry of Unstable and Stable Species, CAS Research/Education Center for Excellence in Molecular Sciences, Institute of Chemistry, Chinese Academy of Sciences, Beijing 100190, China; qiubing@iccas.ac.cn (B.Q.); ww2016@iccas.ac.cn (W.W.)

2   University of Chinese Academy of Sciences, Beijing 100049, China

*   Correspondence: xyang@iccas.ac.cn; Tel.: +86-10-82362928

check for updates

Abstract: Inspired by the active site structures of lactate racemase and recently reported sulphur–carbon–sulphur (SCS) nickel pincer complexes, a series of scorpion-like SCS nickel pincer complexes with an imidazole tail and asymmetric claws was proposed and examined computationally as potential catalysts for the asymmetric transfer hydrogenation of 1-acetonaphthone. Density functional theory calculations reveal a proton-coupled hydride transfer mechanism for the dehydrogenation of (R)-(+)-1-phenyl-ethanol and the hydrogenation of 1-acetonaphthone to produce (R)-(+)-1-(2-naphthyl)ethanol and (S)-(−)-1-(2-naphthyl)ethanol. Among all proposed Ni complexes, **1$_{Ph}$** is the most active one with a rather low free energy barrier of 24 kcal/mol and high enantioselectivity of near 99% enantiomeric excess (*ee*) for the hydrogenation of prochiral ketones to chiral alcohols.

1. Introduction

The synthesis of chiral compounds by metal-catalyzed asymmetric hydrogenation reactions has been widely used in the pharmaceutical [1], agrochemical [2], fragrance [3], and other fine chemical industries [4]. The catalytic asymmetric reduction of prochiral ketones and imines, especially asymmetric hydrogenation (AH) and asymmetric transfer hydrogenation (ATH), is one of the most efficient and versatile tools to produce chiral alcohols and amines. In both academic and industrial operations, catalysts used for AH and ATH are typically based on noble metals, such as Rh, Ir, and Ru [5]. The replacement of such high-cost and toxic precious metals with abundant and environmentally benign base metals, such as Fe, Co, Ni, etc., for catalytic AH and ATH reactions has attracted increasing attention in recent years [6–12]. Gao [9] and Morris [10–12] groups reported tetradentate PNNP iron catalysts for the ATH of acetophenone with high enantioselectivities. Morris and co-workers [13] reported unsymmetrical iron P-NH-P' complexes for the asymmetric hydrogenation of aryl ketones with enantiomeric excess (*ee*) values greater than 90%. In contrast to the encouraging progress archived in iron catalysts, cobalt catalysts for catalytic ATH of ketones have rather low enantioselectivities [9], and only a few Ni catalysts were reported so far [14–16]. In 2008, Hamada et al. [14] applied nickel bisphosphine complexes for the asymmetric hydrogenation of α-amino-β-keto ester hydrochlorides through dynamic kinetic resolution and achieved high diastereo- and enantioselectivities (88−93% *ee*) for the production of anti-β-hydroxy-α-amino esters. Later on, they

applied the same catalyst for the asymmetric hydrogenation of substituted aromatic *α*-aminoketone hydrochlorides to produce *β*-aminoalcohols with excellent diastereo- and enantioselectivities [15]. In 2012, Dong et al. [16] reported Ni(II) complexes chelated by PNO ligands for the ATH of a series of aromatic ketones using 2-propanol as the hydrogen source and obtained corresponding optical alcohols up to 84% *ee* under mild conditions.

Inspired by the structures of the active site of lactate racemase [17] and experimentally reported sulphur–carbon–sulphur (SCS) palladium pincer complexes [18], we recently proposed a series of scorpion-like SCS nickel pincer complexes with an imidazole tail as potential catalysts for lactate racemization [19]. Our density functional theory (DFT) calculations revealed a weak enantioselectivity in the hydrogenation of pyruvate catalyzed by those SCS nickel pincer complexes with unsymmetrical ligands. Based on those findings, we proposed and computationally examined in this work a series of potential unsymmetrical catalysts with enhanced steric effect by adjusting the size of functional groups in the SCS pincer ligand for the more challenging asymmetric transfer hydrogenation of naphthyl ketone.

2. Results and Discussion

Figure 1 shows Meguro et al.'s SCS nickel pincer complexes [18], our previously proposed scorpion-like SCS nickel pincer complex [19], and the unsymmetrical SCS nickel pincer complexes (**1**$_{Ph}$, **1**$_{Me}$, **1**$_{Et}$, and **1**$_{tBu}$) proposed in this study. Scheme 1 shows the catalytic cycles for the ATH of 1-acetonaphthone to (*R*)-(+)-1-(2-naphthyl)ethanol and (*S*)-(−)-1-(2-naphthyl)ethanol catalyzed by catalyst **1**$_{Ph}$. (*R*)-(+)-1-phenyl-ethanol was used as the hydrogen source because the phenyl group in it could have π–π stacking interaction with the phenyl groups in **1**$_{Ph}$ (see Supplementary Materials) and reduce the reaction energy barriers. Actually, both (*R*)-(+)-1-phenyl-ethanol and (*S*)-(−)-1-phenyl-ethanol in racemic (±)-1-phenyl-ethanol could act as hydrogen sources with similar barriers for dehydrogenation. Figure 2 shows the calculated free energy profile of the reaction described in Scheme 1. The optimized structures of some important intermediates and transition states for hydrogen transfer are displayed in Figure 3. The free energy profiles of the same reaction catalyzed by **1**$_{Me}$, **1**$_{Et}$, and **1**$_{tBu}$ are shown in Figures 4–6, respectively.
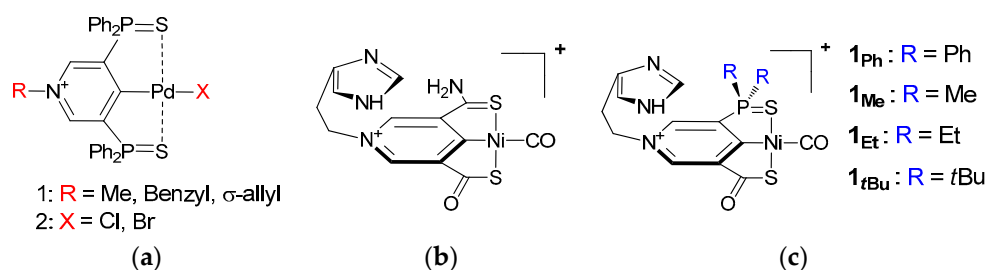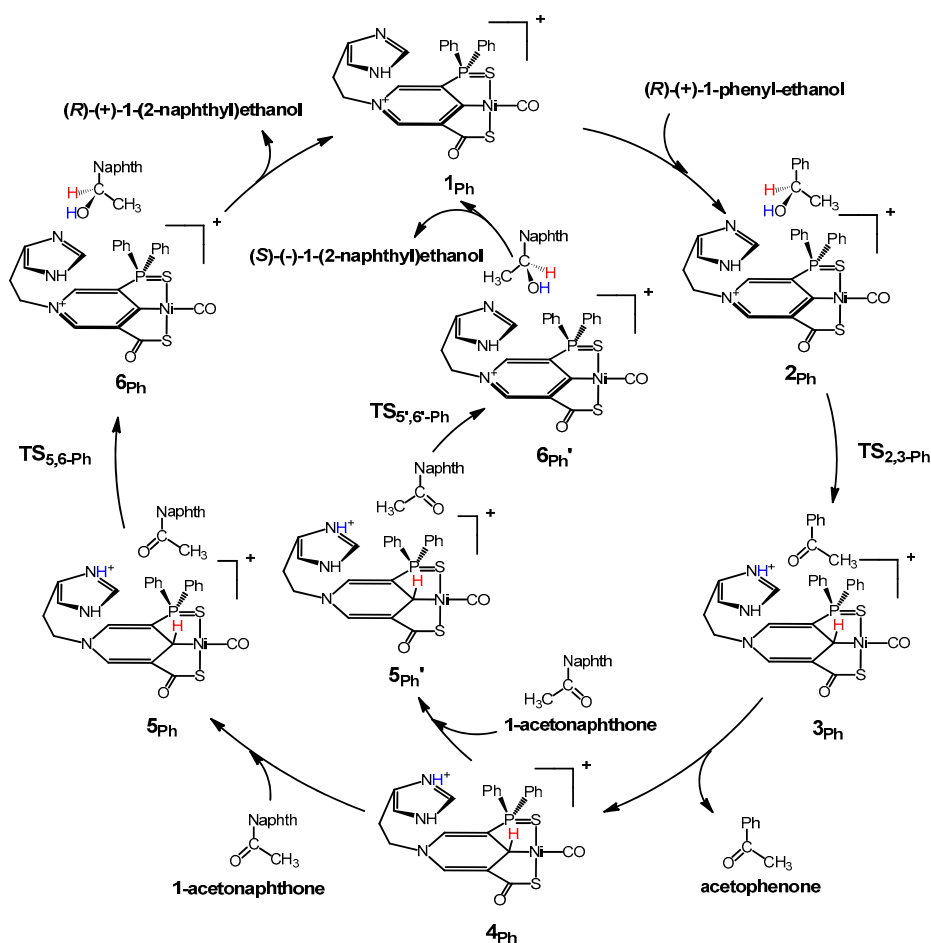

Figure 1. (**a**) Sulphur–carbon–sulphur (SCS) Pd pincer complexes synthesized by Meguro et al.; (**b**) SCS Ni pincer complex designed by Qiu and Yang; (**c**) unsymmetrical SCS pincer complexes proposed in this work.

Scheme 1. Proposed catalytic cycle for the asymmetric transfer hydrogenation of 1-acetonaphthone to (*R*)-(+)-1-(2-naphthyl)ethanol and (*S*)-(−)-1-(2-naphthyl)ethanol catalyzed by **1_{Ph}**.
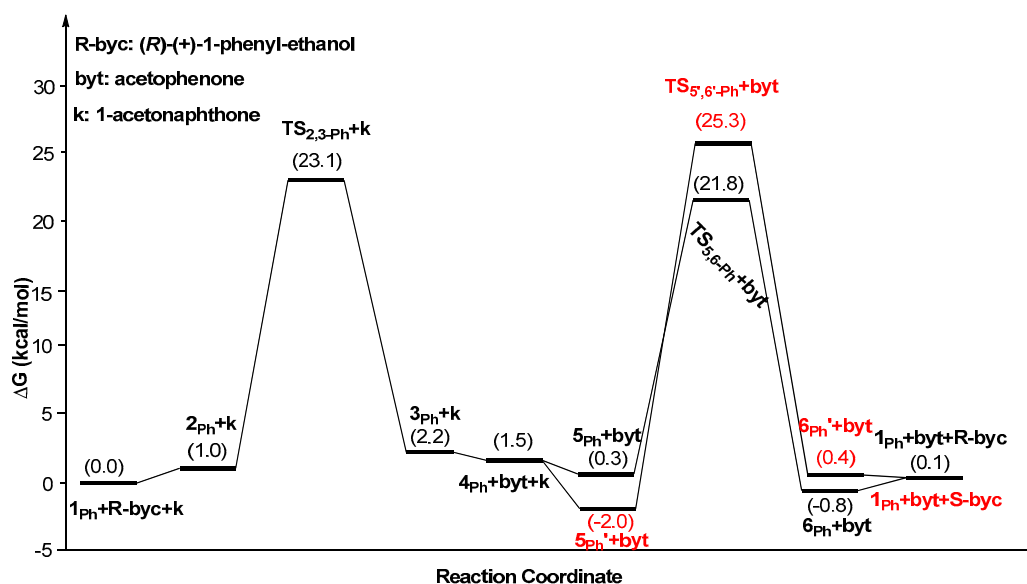

Figure 2. Free energy profile for the asymmetric transfer hydrogenation of 1-acetonaphthone catalyzed by **1_{Ph}**.

At the beginning of the reaction, a (*R*)-(+)-1-phenyl-ethanol molecule approaches **1_{Ph}** and forms a slightly less stable intermediate **2_{Ph}**. The proton and hydride on the hydroxymethyne

group in (*R*)-(+)-1-phenyl-ethanol simultaneously transfer to the imidazole nitrogen and the sp^2 carbon coordinated to nickel, respectively, through transition state **TS$_{2,3\text{-Ph}}$** (ΔG = 23.1 kcal/mol). The dissociation of acetophenone from **3$_{Ph}$** is a 0.7 kcal/mol downhill step. Then, a 1-acetonaphthone molecule approaches the pincer metal complex and forms a 1.2 kcal/mol more stable intermediate **5$_{Ph}$** or a 3.5 kcal/mol more stable intermediate **5$_{Ph}$'**, depending on the orientation of 1-acetonaphthone. The proton and hydride could simultaneously transfer from the pincer ligand in **5$_{Ph}$** or **5$_{Ph}$'** to 1-acetonaphthone through transition state **TS$_{5,6\text{-Ph}}$** or **TS$_{5',6'\text{-Ph}}$** with a free energy barrier of 23.8 (**5$_{Ph}$'**→**TS$_{5,6\text{-Ph}}$**) or 27.3 (**5$_{Ph}$'**→**TS$_{5',6'\text{-Ph}}$**) kcal/mol for the formation of (*R*)-(+)-1-(2-naphthyl)ethanol and (*S*)-(−)-1-(2-naphthyl)ethanol, respectively.
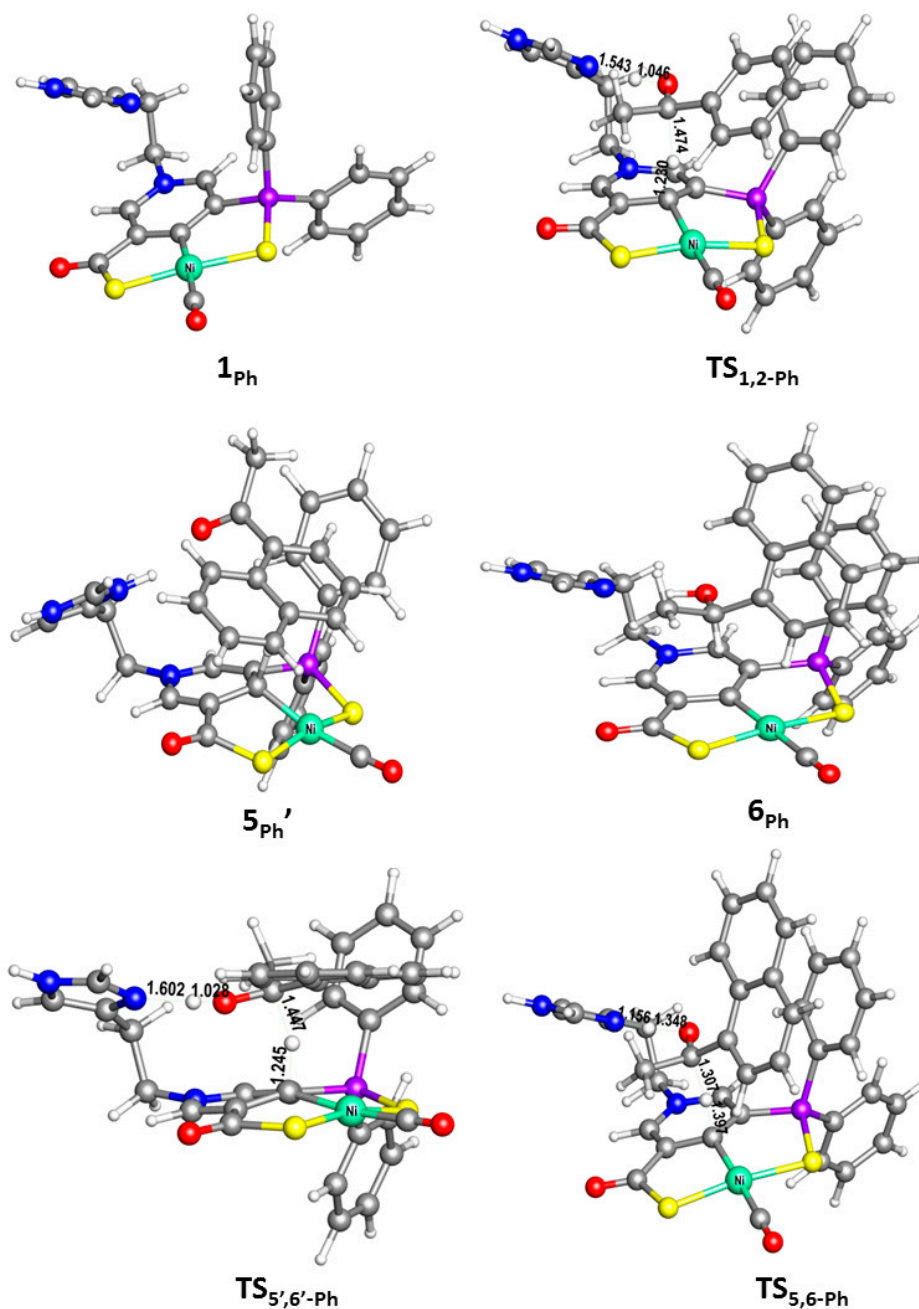

Figure 3. Optimized structure of **1$_{Ph}$**, **TS$_{1,2\text{-Ph}}$** (687*i* cm^{-1}), **5$_{Ph}$'**, **6$_{Ph}$**, **TS$_{5',6'\text{-Ph}}$** (746*i* cm^{-1}), and **TS$_{5,6\text{-Ph}}$** (1099*i* cm^{-1}). Bond lengths are in angstrom. (cyan: Ni, yellow: S, blue: N, red: O, grey: C, white: H)
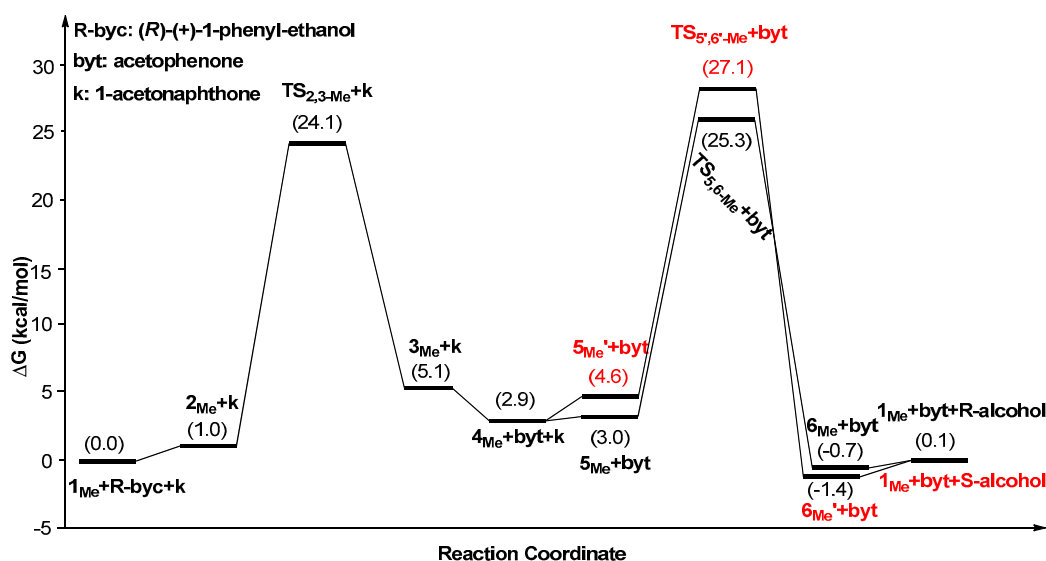
Figure 4. Relative free energy profile for the asymmetric transfer hydrogenation catalyzed by 1_{Me}.
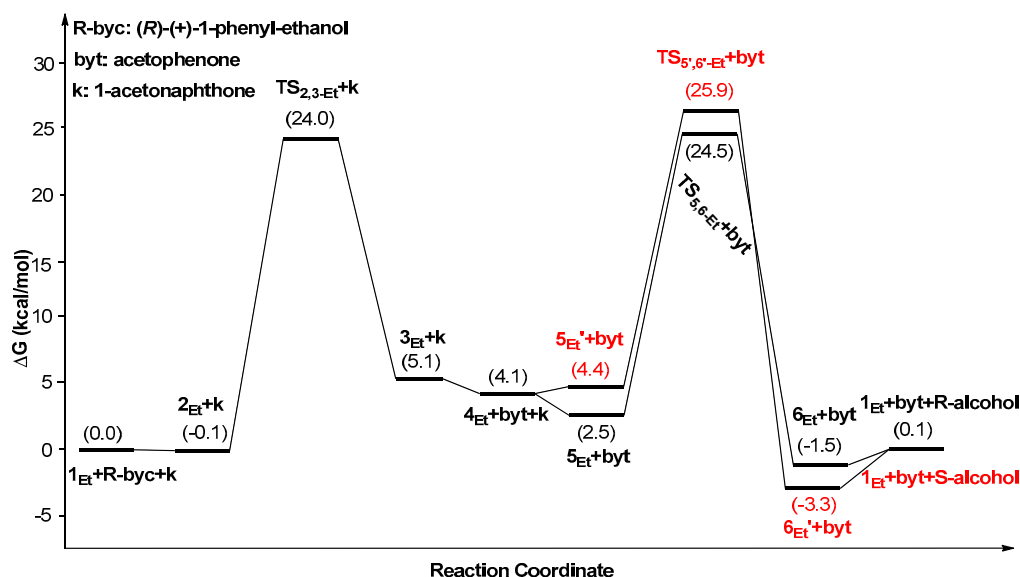

Figure 5. Relative free energy profile for the asymmetric transfer hydrogenation catalyzed by 1_{Et}.

The free energy difference of the enantio-determining steps, $TS_{5,6-Ph}$ and $TS_{5',6'-Ph}$, is 3.5 kcal/mol, which could lead to an approximate *ee* value of 99.5%. The asymmetric transfer hydrogenation of 1-acetonaphthone catalyzed by 1_{Ph}, 1_{Me}, 1_{Et}, and 1_{tBu} has similar mechanisms but different relative energies in the catalytic cycle. Table 1 lists the free energy barriers of the reactions and the enantioselectivity of 1_{Ph}, 1_{Me}, 1_{Et}, and 1_{tBu}. As shown in Table 1, the free energy barrier of the dehydrogenation of (R)-(+)-1-phenyl-ethanol (ΔG_1) catalyzed by 1_{Ph} is 25.1 kcal/mol ($5_{Ph}' \rightarrow TS_{2,3-Ph}$), which is 0.5, 2.3, and 2.8 kcal/mol lower than the ΔG_1 of 1_{Me} ($6_{Me}' \rightarrow TS_{2,3-Me}$), 1_{Et} ($6_{Et}' \rightarrow TS_{2,3-Et}$), and 1_{tBu} ($1_{tBu} \rightarrow TS_{2,3-tBu}$), respectively. The free energy barriers of enantio-determining steps (ΔG_2 and ΔG_3) of 1_{Ph}, 1_{Me}, 1_{Et}, and 1_{tBu} have the same trend. Although 1_{Me}, 1_{Et}, and 1_{tBu} have stronger steric effects than 1_{Ph}, there is a trade-off between their free energy barriers and enantioselectivities. 1_{tBu} has the strongest steric effect, which leads to the highest free energy barrier and the highest enantioselectivity. 1_{Ph} has an enantioselectivity close to 1_{tBu}, and the lowest free energy barriers for hydrogen transfers because of the π–π stack interaction between the naphthyl group in the reactant and the phenyl group in 1_{Ph}.
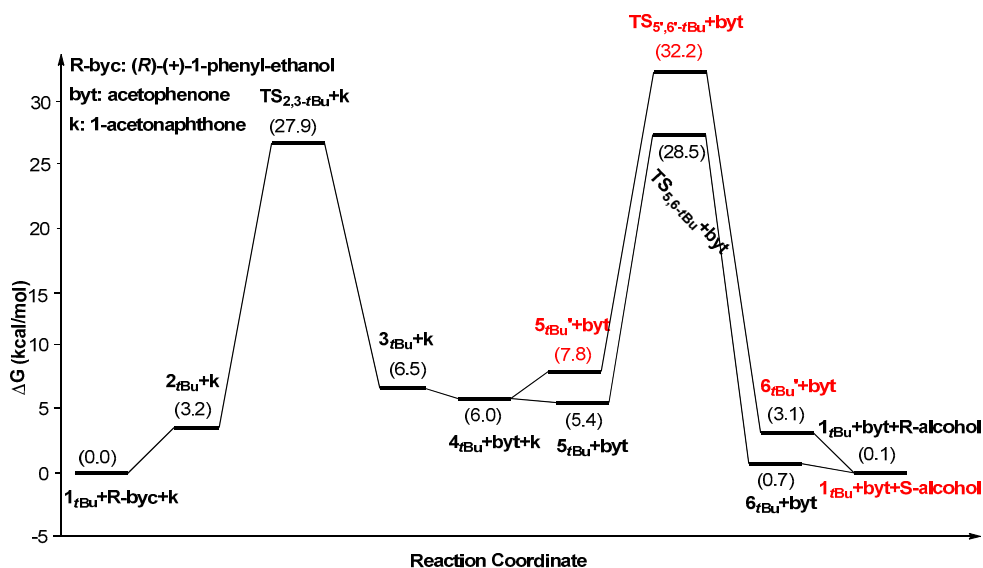
Figure 6. Free energy profile for the asymmetric transfer hydrogenation catalyzed by $1_{t\text{Bu}}$.

Table 1. Energy barriers of 1_{Ph}, 1_{Me}, 1_{Et}, and $1_{t\text{Bu}}$.

Catalysts	ΔG_1 (kcal/mol)	ΔG_2 (kcal/mol)	ΔG_3 (kcal/mol)	$\Delta\Delta G(ee) = \Delta G_2 - \Delta G_3$
1_{Ph}	25.1($5_{\text{Ph}}'\rightarrow\text{TS}_{2,3\text{-Ph}}$)	23.8($5_{\text{Ph}}'\rightarrow\text{TS}_{5,6\text{-Ph}}$)	27.3($5_{\text{Ph}}'\rightarrow\text{TS}_{5',6'\text{-Ph}}$)	−3.5 (99.5%)
1_{Me}	25.6($6_{\text{Me}}'\rightarrow\text{TS}_{2,3\text{-Me}}$)	26.8($6_{\text{Me}}'\rightarrow\text{TS}_{5,6\text{-Me}}$)	28.6($6_{\text{Me}}'\rightarrow\text{TS}_{5',6'\text{-Me}}$)	−1.8 (90.9%)
1_{Et}	27.4($6_{\text{Et}}'\rightarrow\text{TS}_{2,3\text{-Et}}$)	27.9($6_{\text{Et}}'\rightarrow\text{TS}_{5,6\text{-Et}}$)	29.3($6_{\text{Et}}'\rightarrow\text{TS}_{5',6'\text{-Et}}$)	−1.4 (82.8%)
$1_{t\text{Bu}}$	27.9($1_{t\text{Bu}}\rightarrow\text{TS}_{2,3\text{-}t\text{Bu}}$)	28.5($1_{t\text{Bu}}\rightarrow\text{TS}_{5,6\text{-}t\text{Bu}}$)	32.2($1_{t\text{Bu}}\rightarrow\text{TS}_{5',6'\text{-}t\text{Bu}}$)	−3.7 (99.6%)

It is noteworthy that the special role of the imidazole groups in those newly proposed SCS pincer complexes are proton reservoirs facilitating proton-coupled hydride transfer in the dehydrogenation and hydrogenation reactions. The ethylene group connecting the pyridinium ring and the imidazole group ensures the adjustability of the imidazole group's position for easy accepting or donating of protons. The substituents on the arm of the SCS pincer ligand balance the free energy barriers and the enantioselectivity of the ATH reactions.

3. Computational Methods

3.1. DFT Calculation Details

All DFT calculations in this study were performed using the Gaussian 09 (Revision C.01, Gaussion, Inc., Wallingford, CT, USA) suite of Ab Initio programs [20] for the ωB97X-D [21] functional with the all-electron 6-31+G(d,p) basis set for H, C, N, O, S, and P atoms [22–24] and the Stuttgart relativistic effective core potential basis set for Ni (ECP10MDF) [25]. All structures in this paper were optimized in acetonitrile by using the integral equation formalism polarizable continuum model (IEFPCM) [26] with solvation model based on density (SMD) [27] atomic radii solvent corrections. The ground states were confirmed as singlet through comparison with optimized high-spin analogs. An ultrafine integration grid (99,590) was used for numerical integrations. Thermal corrections were calculated within the harmonic potential approximation on optimized structures under T = 298.15 K and 1 atm pressure. Unless otherwise noted, the relative energies reported in the text are Gibbs free energies with solvent effect corrections. The calculated structures were verified to have no imaginary frequency (IF) for all intermediates and only one IF for each transition state. All transition states were also confirmed to connect proper reactants and products by intrinsic reaction coordinate calculations. The JIMP2 molecular visualizing and manipulating program was employed to draw the 3D molecular structures [28].

3.2. Quantitative Estimation of Enantiomeric Excess

The enantiomeric excess can be quantitatively estimated from the free energy barrier difference of enantio-determining steps ($\Delta\Delta G = \Delta G_2 - \Delta G_3$) based on the transation state theory [29]:

$$ee = \frac{e^{-\frac{\Delta\Delta G}{RT}} - 1}{e^{-\frac{\Delta\Delta G}{RT}} + 1} \times 100\%$$

where R is the universal gas constant and T is the absolute temperature of the reaction in calculation (298.15 K in this case).

4. Conclusions

Inspired by the structures of the active center of lactate racemase and some experimentally reported base metal SCS pincer complexes, we proposed a series of scorpion-like SCS pincer nickel complexes 1_{Ph}, 1_{Me}, 1_{Et}, and 1_{tBu} and computationally predicted their potentials as catalysts for the ATH of ketones. Our computational study reveals a proton-coupled hydride transfer dehydrogenation and hydrogenation mechanism, in which the proton and hydride on the hydroxymethyne group in (*R*)-(+)-1-phenyl-ethanol simultaneously transfer to the imidazole nitrogen and the sp^2 carbon coordinated to nickel and then transfer to the carbonyl group in 1-acetonaphthone for the formation of (*R*)-(+)-1-(2-naphthyl)ethanol or (*S*)-(−)-1-(2-naphthyl)ethanol. Among all SCS pincer nickel complexes we proposed, 1_{Ph} has well-balanced catalytic activity ($\Delta G_2 = 23.8$ kcal/mol) and enantioselectivity ($\Delta\Delta G = -3.5$ kcal/mol). We believe the π–π stacking effect between the phenyl groups in reactants and 1_{Ph} helps to stabilize intermediates and reduce energy barriers in the reaction. Our computational design not only provides prototypical SCS nickel pincer complexes as promising catalysts for the asymmetric hydrogenation of 1-acetonaphthone, but also sheds a light on the development of efficient base metal catalysts with high chiral selectivity. The further design of SCS nickel pincer complexes for the asymmetric hydrogenation of various ketones and imines using different hydrogen sources is underway.

Supplementary Materials: The following are available online at http://www.mdpi.com/2073-4344/9/1/101/s1, Table S1: Relative free energies between 1_{tBu} and key transition states calculated by using different density functionals, Table S2: Relative free energies between 1_{tBu} and key transition states in different solvents, Figure S1: Optimized structures and solvent corrected absolute free energies of 1_{Ph} and two conformers with the imidazole group far away from the metal center ($1_{Ph}'$) and on the other side of the pincer ligand close to the PPh$_2$ group ($1_{Ph}''$).

Conflicts of Interest: The authors declare no conflict of interest.

References

1. Hansen, K.B.; Hsiao, Y.; Xu, F.; Rivera, N.; Clausen, A.; Kubryk, M.; Krska, S.; Rosner, T.; Simmons, B.; Balsells, J.; et al. Highly Efficient Asymmetric Synthesis of Sitagliptin. *J. Am. Chem. Soc.* **2009**, *131*, 8798–8804. [CrossRef] [PubMed]

2. Blaser, H.U.; Pugin, B.; Spindler, F.; Thommen, M. From a Chiral Switch to a Ligand Portfolio for Asymmetric Catalysis. *Acc. Chem. Res.* **2007**, *40*, 1240–1250. [CrossRef] [PubMed]

3. Saudan, L.A. Hydrogenation Processes in the Synthesis of Perfumery Ingredients. *Acc. Chem. Res.* **2007**, *40*, 1309–1319. [CrossRef]

4. Blaser, H.U.; Malan, C.; Pugin, B.; Spindler, F.; Steiner, H.; Studer, M. Selective Hydrogenation for Fine Chemicals: Recent Trends and New Developments. *Adv. Synth. Catal.* **2003**, *345*, 103–151. [CrossRef]

5. Wang, D.; Astruc, D. The Golden Age of Transfer Hydrogenation. *Chem. Rev.* **2015**, *115*, 6621–6686. [CrossRef] [PubMed]

6. Gopalaiah, K. Chiral Iron Catalysts for Asymmetric Synthesis. *Chem. Rev.* **2013**, *113*, 3248–3296. [CrossRef]

7. Pellissier, H.; Clavier, H. Enantioselective Cobalt-Catalyzed Transformations. *Chem. Rev.* **2014**, *114*, 2775–2823. [CrossRef]

8. Morris, R.H. Exploiting Metal-Ligand Bifunctional Reactions in the Design of Iron Asymmetric Hydrogenation Catalysts. *Acc. Chem. Res.* **2015**, *48*, 1494–1502. [CrossRef] [PubMed]

9. Li, Y.Y.; Yu, S.L.; Shen, W.Y.; Gao, J.X. Iron-, Cobalt-, and Nickel-Catalyzed Asymmetric Transfer Hydrogenation and Asymmetric Hydrogenation of Ketones. *Acc. Chem. Res.* **2015**, *48*, 2587–2598. [CrossRef]

10. Zuo, W.W.; Lough, A.J.; Li, Y.F.; Morris, R.H. Amine(imine)diphosphine Iron Catalysts for Asymmetric Transfer Hydrogenation of Ketones and Imines. *Science* **2013**, *342*, 1080–1083. [CrossRef]

11. Zuo, W.W.; Morris, R.H. Synthesis and Use of an Asymmetric Transfer Hydrogenation Catalyst Based on Iron(II) for the Synthesis of Enantioenriched Alcohols and Amines. *Nat. Protoc.* **2015**, *10*, 241–257. [CrossRef] [PubMed]

12. Zuo, W.W.; Prokopchuk, D.E.; Lough, A.J.; Morris, R.H. Details of the Mechanism of the Asymmetric Transfer Hydrogenation of Acetophenone Using the Amine(imine)diphosphine Iron Precatalyst: The Base Effect and the Enantiodetermining Step. *ACS Catal.* **2016**, *6*, 301–314. [CrossRef]

13. Smith, S.A.M.; Lagaditis, P.O.; Lupke, A.; Lough, A.J.; Morris, R.H. Unsymmetrical Iron P-NH-P′ Catalysts for the Asymmetric Pressure Hydrogenation of Aryl Ketones. *Chem. Eur. J.* **2017**, *23*, 7212–7216. [CrossRef] [PubMed]

14. Hamada, Y.; Koseki, Y.; Fujii, T.; Maeda, T.; Hibino, T.; Makino, K. Catalytic Asymmetric Hydrogenation of α-Amino-β-Keto Ester Hydrochlorides Using Homogeneous Chiral Nickel-Bisphosphine Complexes through DKR. *Chem. Commun.* **2008**, *0*, 6206–6208. [CrossRef] [PubMed]

15. Hibino, T.; Makino, K.; Sugiyama, T.; Hamada, Y. Homogeneous Chiral Nickel-Catalyzed Asymmetric Hydrogenation of Substituted Aromatic α-Aminoketone Hydrochlorides through Dynamic Kinetic Resolution. *ChemCatChem* **2009**, *1*, 237–240. [CrossRef]

16. Dong, Z.R.; Li, Y.Y.; Yu, S.L.; Sun, G.S.; Gao, J.X. Asymmetric Transfer Hydrogenation of Ketones Catalyzed by Nickel Complex with New PNO-Type Ligands. *Chin. Chem. Lett.* **2012**, *23*, 533–536. [CrossRef]

17. Desguin, B.; Zhang, T.; Soumillion, P.; Hols, P.; Hu, J.; Hausinger, R.P. A Tethered Niacin-Derived Pincer Complex with a Nickel-Carbon Bond in Lactate Racemase. *Science* **2015**, *349*, 66–69. [CrossRef]

18. Meguro, H.; Koizumi, T.; Yamamoto, T.; Kanbara, T. Synthesis, Structure, and Quaternization and Complexation Reactions of κ3SCS Pincer Palladium Complexes Having 3,5-Pyridinediyl Unit. *J. Organomet. Chem.* **2008**, *693*, 1109–1116. [CrossRef]

19. Qiu, B.; Yang, X.Z. A Bio-Inspired Design and Computational Prediction of Scorpion-Like SCS Nickel Pincer Complexes for Lactate Racemization. *Chem. Commun.* **2017**, *53*, 11410–11413. [CrossRef]

20. Frisch, M.J.; Trucks, G.W.; Schlegel, H.B.; Scuseria, G.E.; Robb, M.A.; Cheeseman, J.R.; Scalmani, G.; Barone, V.; Mennucci, B.; Petersson, G.A.; et al. *Gaussian 09, Revision C.01*; Gaussian, Inc.: Wallingford, CT, USA, 2010.

21. Chai, J.D.; Head-Gordon, M. Long-Range Corrected Hybrid Density Functionals with Damped Atom-Atom Dispersion Corrections. *Phys. Chem. Chem. Phys.* **2008**, *10*, 6615–6620. [CrossRef]

22. Hehre, W.J.; Ditchfield, R.; Pople, J.A. Self-Consistent Molecular Orbital Methods. XII. Further Extensions of Gaussian-Type Basis Sets for Use in Molecular Orbital Studies of Organic Molecules. *J. Chem. Phys.* **1972**, *56*, 2257–2261. [CrossRef]

23. Hariharan, P.C.; Pople, J.A. The Influence of Polarization Functions on Molecular Orbital Hydrogenation Energies. *Theor. Chim. Acta* **1973**, *28*, 213–222. [CrossRef]

24. Francl, M.M.; Pietro, W.J.; Hehre, W.J.; Binkley, J.S.; Gordon, M.S.; DeFrees, D.J.; Pople, J.A. Self-Consistent Molecular Orbital Methods. XXIII. A Polarization-Type Basis Set for Second-Row Elements. *J. Chem. Phys.* **1982**, *77*, 3654–3665. [CrossRef]

25. Martin, J.M.L.; Sundermann, A. Correlation Consistent Valence Basis Sets for Use with the Stuttgart-Dresden-Bonn Relativistic Effective Core Potentials: The Atoms Ga-Kr and In-Xe. *J. Chem. Phys.* **2001**, *114*, 3408–3420. [CrossRef]

26. Tomasi, J.; Mennucci, B.; Cammi, R. Quantum Mechanical Continuum Solvation Models. *Chem. Rev.* **2005**, *105*, 2999–3094. [CrossRef]

27. Marenich, A.V.; Cramer, C.J.; Truhlar, D.G. Universal Solvation Model Based on Solute Electron Density and on a Continuum Model of the Solvent Defined by the Bulk Dielectric Constant and Atomic Surface Tensions. *J. Phys. Chem. B* **2009**, *113*, 6378–6396. [CrossRef]

28. Manson, J.; Webster, C.E.; Hall, M.B. *JIMP2, Version 0.091, A Free Program for Visualizing and Manipulating Molecules*; Texas A&M University: College Station, TX, USA, 2006.

29. Scheneebeli, S.T.; Hall, M.L.; Breslow, R.; Friesner, R. Quantitative DFT Modeling of the Enantiomeric Excess for Dioxirane-Catalyzed Epoxidations. *J. Am. Chem. Soc.* **2009**, *131*, 3965–3973. [CrossRef]